Restored glial glutamate transporter EAAT2 function as a potential therapeutic approach for Alzheimer's disease

Kou Takahashi,[1]* Qiongman Kong,[1]* Yuchen Lin,[1] Nathan Stouffer,[1] Delanie A. Schulte,[1] Liching Lai,[1] Qibing Liu,[1] Ling-Chu Chang,[1] Sky Dominguez,[1] Xuechao Xing,[2] Gregory D. Cuny,[2,3] Kevin J. Hodgetts,[2] Marcie A. Glicksman,[2] and Chien-Liang Glenn Lin[1]

[1]Department of Neuroscience, The Ohio State University, Columbus, OH 43210
[2]Laboratory for Drug Discovery in Neurodegeneration, Harvard NeuroDiscovery Center, Brigham and Women's Hospital and Harvard Medical School, Boston, MA 02115
[3]Department of Pharmacological and Pharmaceutical Sciences, University of Houston College of Pharmacy, Houston, TX 77004

Glutamatergic systems play a critical role in cognitive functions and are known to be defective in Alzheimer's disease (AD) patients. Previous literature has indicated that glial glutamate transporter EAAT2 plays an essential role in cognitive functions and that loss of EAAT2 protein is a common phenomenon observed in AD patients and animal models. In the current study, we investigated whether restored EAAT2 protein and function could benefit cognitive functions and pathology in $APP_{Sw,Ind}$ mice, an animal model of AD. A transgenic mouse approach via crossing EAAT2 transgenic mice with $APP_{Sw,Ind.}$ mice and a pharmacological approach using a novel EAAT2 translational activator, LDN/OSU-0212320, were conducted. Findings from both approaches demonstrated that restored EAAT2 protein function significantly improved cognitive functions, restored synaptic integrity, and reduced amyloid plaques. Importantly, the observed benefits were sustained one month after compound treatment cessation, suggesting that EAAT2 is a potential disease modifier with therapeutic potential for AD.

CORRESPONDENCE
Chien-Liang Glenn Lin:
lin.492@osu.edu

Abbreviations used: AD, Alzheimer's disease; DHK, dihydrokainic acid; LTP, long-term potentiation; PMV, plasma membrane vesicle.

Glutamatergic neurons located in the hippocampus and the frontal, temporal, and parietal cortices are severely affected in Alzheimer's disease (AD) patients (Braak and Braak, 1998; Francis, 2003). A study investigating changes in the glutamatergic system in AD brains indicates that cognitive deficits are more significantly correlated with reduced glutamatergic presynaptic bouton density than with neurofibrillary tangles or amyloid β burden (Bell et al., 2007). Deficiencies in many stages of the glutamate cycle, including reduced glutamate uptake function, have been reported in AD and are correlated with cognitive decline (Masliah et al., 1996; Kirvell et al., 2006; Jacob et al., 2007; Kashani et al., 2008; Scott et al., 2011; Sokolow et al., 2012). Reduced glutamate uptake function can lead to increased extracellular glutamate levels, which, after long periods of time, can potentially increase amyloid β production, as shown in previous studies (Lesné et al., 2005; Bordji et al., 2010; Kim et al., 2010). Amyloid β has been reported to further induce glutamate release (Chin et al., 2007; Kabogo et al., 2010; Talantova et al., 2013), thus exacerbating glutamate levels. Moreover, amyloid β has been demonstrated to inhibit induction of long-term potentiation (LTP) and promote long-term depression (Wang et al., 2004; Li et al., 2009, 2011; Shankar et al., 2008). This amyloid β–facilitated long-term depression can be prevented by an extracellular glutamate scavenger (Li et al., 2009). Current literature suggests that homeostatic regulation of extracellular glutamate levels may play a crucial role in the pathogenesis of AD.

*K. Takahashi and Q. Kong contributed equally to this paper.

The Rockefeller University Press $30.00
J. Exp. Med. 2015 Vol. 212 No. 3 319–332
www.jem.org/cgi/doi/10.1084/jem.20140413

The Journal of Experimental Medicine

Excitatory amino acid transporter 2 (EAAT2) plays a critical role in the maintenance of low extracellular glutamate levels. EAAT2 is primarily localized in perisynaptic processes of astrocytes closely associated with excitatory synaptic contacts (Chaudhry et al., 1995; Rothstein et al., 1996; Lin et al., 2012). Previous literature has indicated that loss of EAAT2 protein and function are commonly found in AD patients (Masliah et al., 1996; Jacob et al., 2007; Scott et al., 2011) and are an early event in disease pathology. Although the mechanisms underlying the loss of EAAT2 remain unclear, a previous study has demonstrated that this loss is probably caused by disturbances at the posttranscriptional level because EAAT2 mRNA is not decreased (Li et al., 1997). To determine whether the loss of EAAT2 contributes to AD, Mookherjee et al. (2011) crossed mice lacking one allele for EAAT2 with AβPPswe/PS1ΔE9 mice and found accelerated cognitive deficits in the crossed mice. These findings suggest that decreased EAAT2 levels may contribute to AD.

In the present study, we aimed to investigate whether restored EAAT2 protein levels and function could ameliorate AD-like behavior and pathology in mice and whether EAAT2 is a potential therapeutic target for AD. These aims were assessed using transgenic mice and pharmacological approaches. First, EAAT2 transgenic mice having a 1.5–2-fold increase in EAAT2 protein levels (Guo et al., 2003) were crossed with $APP_{Sw,Ind}$ mice (Mucke et al., 2000). The crossed mice exhibited restored EAAT2 protein levels and function and, most importantly, significantly improved cognitive functions, restored synaptic integrity, and reduced amyloid plaques. Next, $APP_{Sw,Ind}$ mice were treated with a novel brain-penetrant small molecule, LDN/OSU-0212320, which we previously identified as capable of increasing EAAT2 expression through translational activation (Colton et al., 2010; Xing et al., 2011; Kong et al., 2014). Significantly, we found that this compound can restore EAAT2 function and ameliorate AD-like behavior and pathology, thus having therapeutic potential for AD.

RESULTS

Increased EAAT2 protects against Aβ-induced neuronal damage in primary cultures

As a first step, we investigated whether increased EAAT2 protein expression could prevent $Aβ_{25-35}$ oligomer–induced neuronal toxicity in primary neuron and astrocyte mixed cultures. Cultures were prepared from EAAT2 transgenic pups that expressed ∼1.5–2-fold more EAAT2 than their nontransgenic WT littermates (Guo et al., 2003). 7-d-old cultures were treated with 40 μM $Aβ_{25-35}$ oligomers, and at 24 h, EAAT2 protein levels were determined by Western blot analysis. Results showed about a 45% decrease in EAAT2 protein levels in Aβ-treated nontransgenic cultures and only about a 5.3% decrease in treated EAAT2 transgenic cultures (Fig. 1 A). It is notable that data can only be compared between treated and nontreated cultures prepared from the same pup brain; i.e., nontransgenic cultures cannot be compared with transgenic cultures. We also measured glutamate uptake activities by [^{3}H]glutamate uptake assay. Dihydrokainic acid (DHK), an EAAT2 blocker, was used to distinguish EAAT2-mediated glutamate uptake from uptake mediated by the other EAATs. Results showed that total Na^+-dependent [^{3}H]glutamate uptake activity (fmol/mg protein/min) was decreased ∼12% in treated nontransgenic cultures (−Aβ: 175.9 ± 17.64 vs. +Aβ: 156.5 ± 19.81) and not decreased in treated transgenic cultures (−Aβ: 257.4 ± 10.16 vs. +Aβ: 258.0 ± 9.90; Fig. 1 B, left; and Table S1). The DHK-sensitive [^{3}H]glutamate uptake activity (fmol/mg protein/min) was decreased ∼60% in treated nontransgenic cultures (−Aβ: 33.8 ± 1.99 vs. +Aβ: 12.6 ± 2.49) and ∼16% in treated transgenic cultures (−Aβ: 42.8 ± 3.88 vs. +Aβ: 35.8 ± 1.76; Fig. 1 B, right; and Table S1). To evaluate the effects of increased EAAT2 on $Aβ_{25-35}$-induced neuronal toxicity, we visualized neuronal morphology by immunostaining with MAP2 antibodies. Profound neuronal damage, specifically neurite degeneration, was observed in $Aβ_{25-35}$-treated nontransgenic cultures, whereas neurons in EAAT2 transgenic cultures were spared (representative images shown in Fig. 1 C). Importantly, the observed protective effects were abolished in the presence of DHK, indicating that the effects were caused by increased EAAT2 function (Fig. 1 C). DHK treatment alone did not cause neuronal damage as assessed by neuronal morphology, neuronal number, and number of dying neurons in the form of condensed nuclei (not depicted). To further quantify our observations, we counted the number of MAP2-positive neurons and found that $Aβ_{25-35}$ treatment did not decrease neuronal number in both transgenic cultures (547 neurons/2.2 mm^2 without Aβ vs. 555 neurons/2.2 mm^2 with Aβ, averaged across four experiments) and nontransgenic cultures (535 neurons/2.2 mm^2 without Aβ vs. 550 neurons/2.2 mm^2 with Aβ, averaged across five experiments). After, we counted MAP2-positive neurons with condensed nuclei stained by Hoechst 33342. The results showed that $Aβ_{25-35}$ treatment increased the number of neurons with condensed nuclei by 36% in nontransgenic cultures but only 6% in transgenic cultures. Significantly, when DHK was used to block EAAT2 function, the number of neurons with condensed nuclei in treated transgenic cultures increased by 39%, as observed in nontransgenic cultures (Fig. 1 D). Furthermore, we quantified the intensity of MAP2 immunoreactivity as an indicator of neurite degeneration and found that $Aβ_{25-35}$ treatment decreased MAP2 immunoreactivity by 30% in nontransgenic cultures but only 5% in transgenic cultures (Fig. 1 E). In the presence of DHK, MAP2 immunoreactivity was significantly decreased by 33% in $Aβ_{25-35}$-treated transgenic cultures, as observed in nontransgenic cultures. These results indicate that increased EAAT2 expression and function protects against $Aβ_{25-35}$-induced neuronal damage in the presented in vitro culture model.

EAAT2 protein was restored in $APP_{Sw,Ind}$-crossed EAAT2 mice

To determine whether the observed protective effects in primary cultures are present in an AD animal model, we crossed our EAAT2 mice with $APP_{Sw,Ind}$ mice to increase EAAT2 protein expression levels. We previously reported that $APP_{Sw,Ind}$ mice, at the age of 9 mo, when disease and pathology are evident, exhibited an ∼40% loss of EAAT2 protein expression as

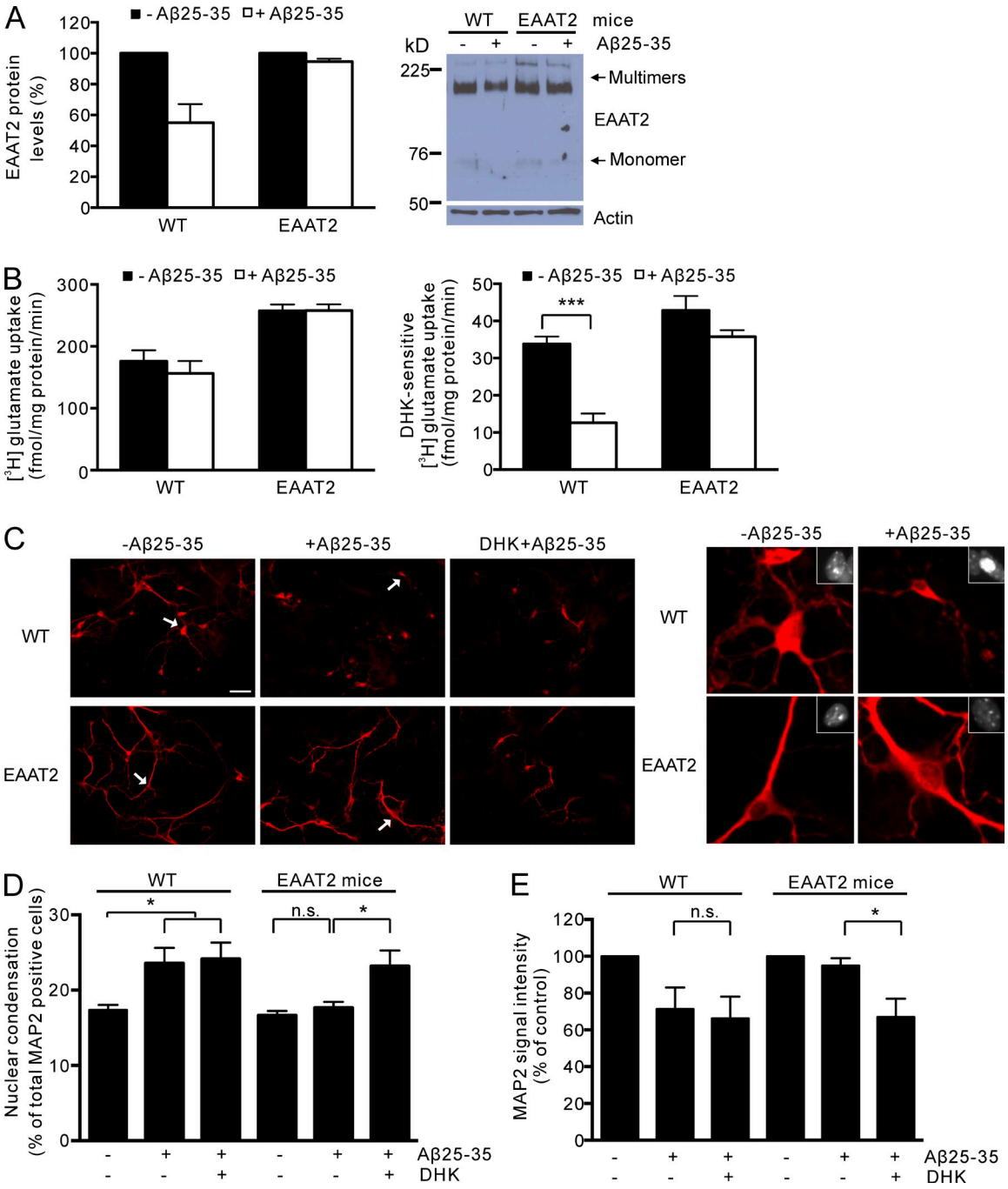

Figure 1. Increased EAAT2 expression significantly protected against $A\beta_{25-35}$-induced neuronal damage in primary cultures. Cortical primary neuron and astrocyte mixed cultures were prepared from EAAT2 transgenic or WT pup littermates. 7-d-old primary cultures were treated with 40 µM $A\beta_{25-35}$ for 24 h. (A) Quantitative analysis of EAAT2 protein levels in $A\beta_{25-35}$-treated and nontreated cultures by Western blotting. Representative Western blot result is shown. EAAT2 signal intensity was normalized to its actin signal intensity on the same blot. It is notable that data can only be compared between treated and nontreated cultures prepared from the same pup brains ($n = 4$). (B) Glutamate uptake analysis. Left panel is total [^{3}H]glutamate uptake, and right panel is DHK-sensitive [^{3}H]glutamate uptake ($n = 4–5$; ***, $P < 0.001$, Student's t test). Raw data are presented in Table S1. (C) Representative images of immunocytochemistry staining with MAP2 and Hoechst 33342 showing neurite degeneration and nuclear condensation. The neurons indicated with arrows are magnified in the images on the right. The nuclear staining is represented in the insets. Bar, 50 µm. (D) Quantitative analysis of the number of neurons showing condensed nuclei. Approximately 500 neurons per culture were evaluated as the percentage of neurons showing condensed nuclei, and four to five cultures per group were statistically analyzed (*, $P < 0.05$, one way ANOVA followed by Holm-Šídák method). (E) Quantitative analysis of MAP2 immunoreactivity. A total of 2.2-mm^2 area per culture was evaluated, and the mean intensity of no treatment samples was arbitrarily set as 100%. Four to five cultures per group were statistically analyzed (*, $P < 0.05$, one way ANOVA followed by Holm-Šídák method). All data are from three independent experiments. Mean ± SEM is shown.

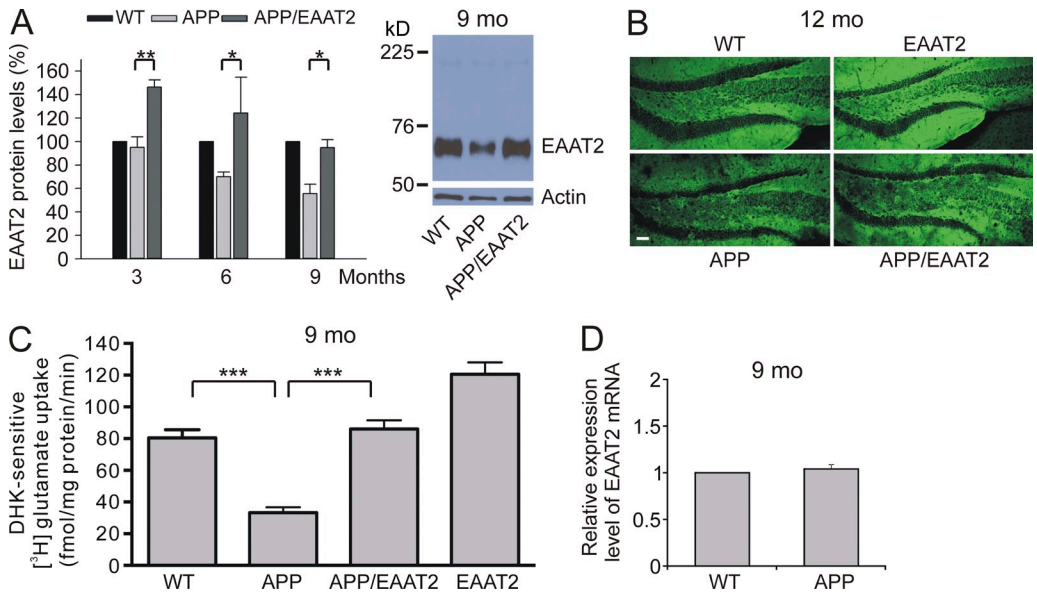

Figure 2. Functional EAAT2 protein was restored in APP/EAAT2 mice. (A) Quantitative analysis of EAAT2 protein levels in the forebrain of the indicated mice. EAAT2 protein levels for each sample were normalized to actin protein levels ($n = 6$; *, $P < 0.05$; **, $P < 0.01$, Student's *t* test). Representative Western blot analysis of EAAT2 protein levels at 9 mo of age is shown. (B) Representative images of EAAT2 immunofluorescent staining for 12-mo-old mice in the hippocampal dentate gyrus region ($n = 3$). Bar, 50 µm. (C) DHK-sensitive [^{3}H]glutamate uptake activity ($n = 3$; ***, $P < 0.001$, one way ANOVA followed by Holm-Šídák method). PMVs prepared from mouse forebrains were used for glutamate uptake measurement. (D) EAAT2 mRNA levels in the forebrain of the indicated mice measured by real-time RT-PCR analysis ($n = 6$). Data are from six (A and D) and three (B and C) independent experiments. Mean ± SEM is shown.

compared with their WT littermates (Tian et al., 2010). Crossed mice were evaluated for EAAT2 protein levels and glutamate uptake function at 3, 6, and 9 mo of age. As shown in Fig. 2 A, EAAT2 protein expression decreased with age in $APP_{Sw,Ind}$ mice, whereas at 9 mo of age, EAAT2 protein levels in the APP/EAAT2 mice remained similar to that of the WT mice. Even at 12 mo of age, the APP/EAAT2 mice exhibited similar EAAT2 protein levels as their nontransgenic littermates in the hippocampus area (Fig. 2 B). Consistent with EAAT2 protein expression, DHK-sensitive [^{3}H]glutamate uptake function was restored in APP/EAAT2 mice at 9 mo (Fig. 2 C; WT: 80.5 ± 5.03, APP: 33.3 ± 3.36, APP/EAAT2: 86.0 ± 5.57, and EAAT2: 120.6 ± 7.43 fmol/mg protein/min). We measured EAAT2 mRNA levels by quantitative RT-PCR analysis and found that EAAT2 mRNA levels did not decrease in $APP_{Sw,Ind}$ mice, suggesting that loss of EAAT2 protein is not caused by decreased mRNA levels (Fig. 2 D). These observed phenomena are similar to that reported in AD patients (Li et al., 1997). It is notable that total APP protein expression was not different in APP/EAAT2 mice compared with their $APP_{Sw,Ind}$ littermates (not depicted).

Improved cognitive functions and reduced AD-like pathology in APP/EAAT2 mice

To assess the potential benefits of increased EAAT2 protein expression, we investigated cognitive functions and pathological changes in crossed mice compared with their $APP_{Sw,Ind}$ littermates. Previous literature has indicated that several lines of APP mice exhibit network hyperexcitability, spontaneous epileptiform activity, and an abnormally high rate of premature death (Hsiao et al., 1995; Palop et al., 2007; Minkeviciene et al., 2009; Verret et al., 2012). AD patients also have a high incidence of seizures and epilepsy (Friedman et al., 2012). We monitored these phenomena in $APP_{Sw,Ind}$ and APP/EAAT2 mice. We found that by the age of 100 d, $APP_{Sw,Ind}$ and APP/EAAT2 mice showed accelerated mortality compared with WT, with 36% and 17% death rates, respectively (Fig. 3 A); APP/EAAT2 mice exhibited significantly lowered premature death rates ($P < 0.05$, χ^2 test). No marked weight loss, malformations of the vital organs, or major internal bleeding were associated with premature death. Seizure activity was observed and could have contributed to the premature death rate.

Next, we examined cognitive functions at 12–14 mo of age. Y-maze tests were conducted to assess short-term memory. Results revealed that APP/EAAT2 mice exhibited significantly improved spontaneous alternations compared with their $APP_{Sw,Ind}$ littermates (Fig. 3 B). T-maze was then conducted to assess spatial learning memory. Results showed that APP/EAAT2 mice exhibited significantly better spatial learning memory ability than their $APP_{Sw,Ind}$ littermates (Fig. 3 C). These results were not the result of side preference effects because side preference was controlled for in the procedure, as described in Materials and methods. To assess nonspatial long-term memory, novel object recognition tests were performed. As found with the other cognitive tests, it was determined that APP/EAAT2 mice had significantly improved novel object recognition memory as compared with their $APP_{Sw,Ind}$ littermates (Fig. 3 D). Interestingly, there was a tendency for

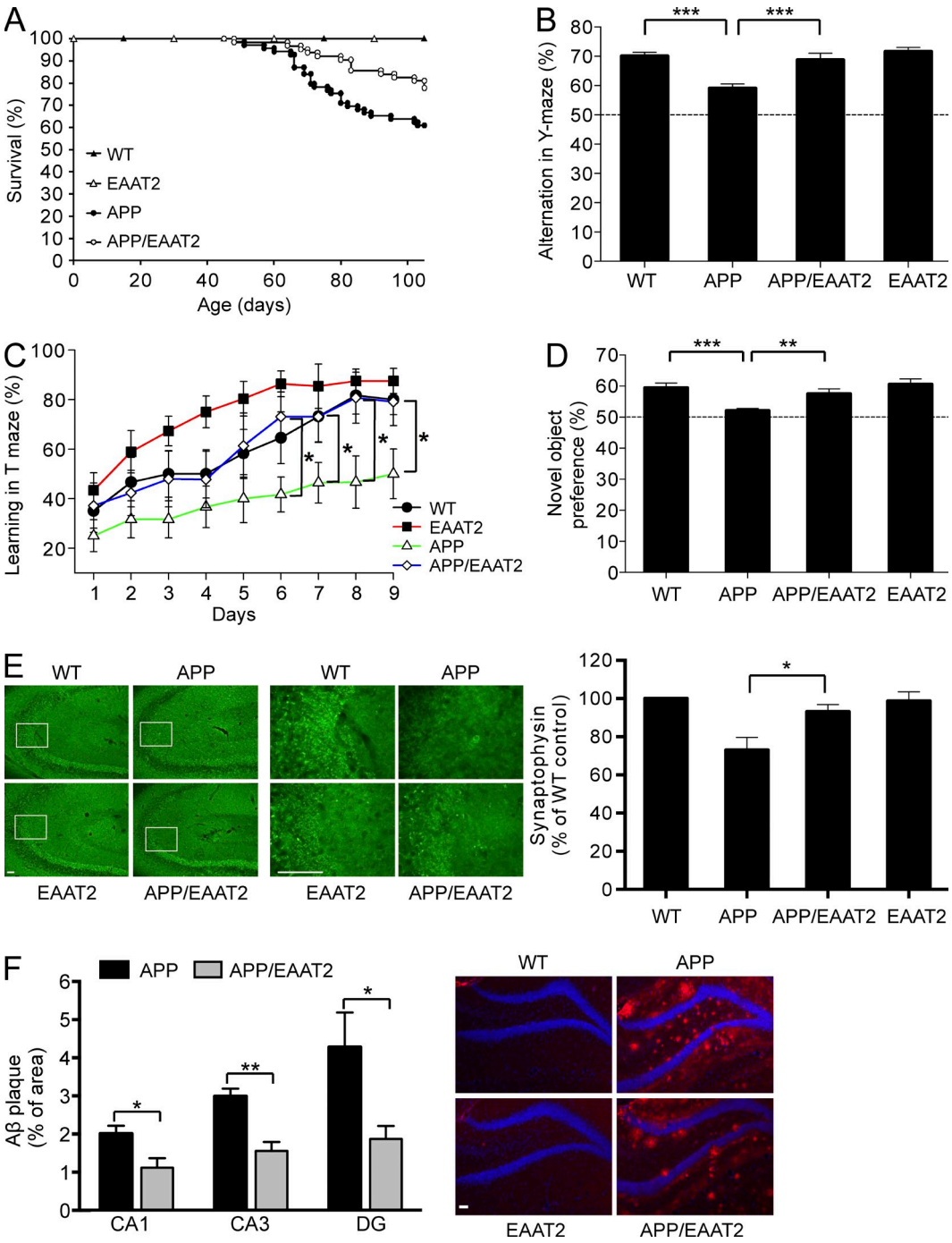

Figure 3. APP/EAAT2 mice exhibited improved premature death rate, memory, and pathology compared with their APP littermates. (A) Survival curves were generated from 246 mice: 63 APP/EAAT2, 69 $APP_{Sw,Ind}$, 59 EAAT2, and 55 WT littermates. (B–D) Behavior tests were conducted in 12–14-mo-old mice (n = 14–17 per group). (B) Y-maze tests assessing short-term memory (***, $P < 0.001$, one way ANOVA followed by Holm-Šídák method). The dotted line represents the point at which mice did not remember the previously visited arm. (C) T-maze tests assessing spatial learning memory (*, $P < 0.05$, one-way repeated ANOVA followed by Student's t tests). (D) Novel object recognition tests assessing long-term nonspatial memory (**, $P < 0.01$; ***, $P < 0.001$, one way ANOVA followed by Holm-Šídák method). The dotted line represents the point at which mice did not remember the previous object. (E, left) Representative images of synaptophysin immunostaining in the CA3 region. The right micrographs show high-magnification images of the boxed areas in the left micrographs. (right) Quantitative analysis of synaptophysin immunoreactivity in the CA3a region indicated by the boxed areas (n = 3–5 mice per group; *, $P < 0.05$, Student's t test). (F, left) Quantitative analysis of Aβ immunostaining (n = 4–5 mice per group; *, $P < 0.05$; **, $P < 0.01$, Student's t test). (right) Representative images of Aβ immunostaining in the dentate gyrus region are shown. Nuclei were stained with Hoechst 33342 (blue). (E and F) Bars, 50 µm. Data are from six (A), four (B–D), and three (E and F) independent experiments. Mean ± SEM is shown.

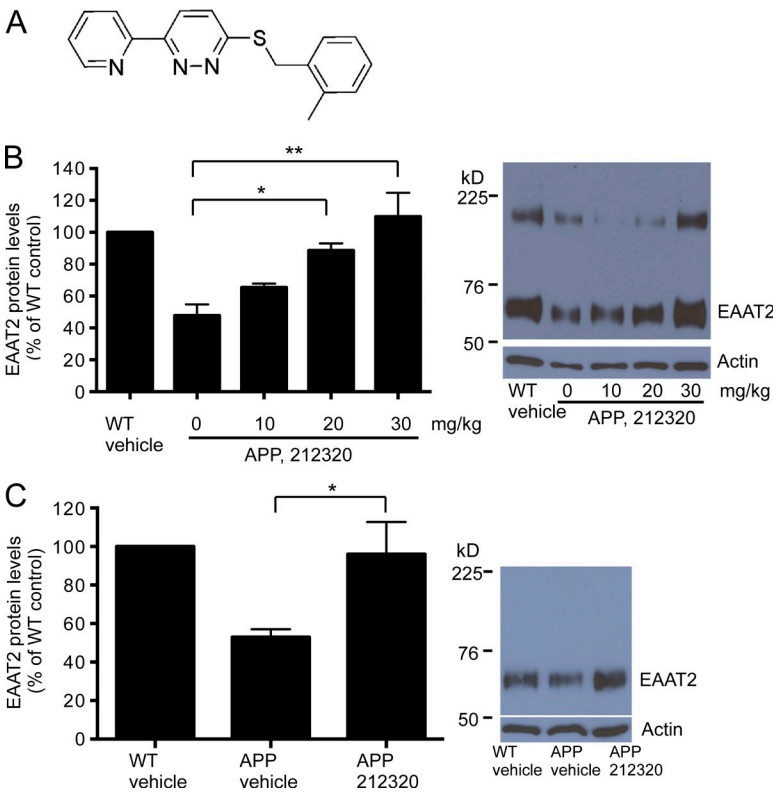

Figure 4. EAAT2 protein levels were restored by LDN/OSU-0212320 in 12-mo-old $APP_{Sw,Ind}$ mice. (A) Structure of LDN/OSU-0212320. (B) 12-mo-old $APP_{Sw,Ind}$ mice were treated with the indicated dosages of compound by i.p. injection for 3 d. PMVs were prepared from forebrains to determine EAAT2 protein levels by Western blot analysis. EAAT2 signal intensity was normalized to its actin signal intensity on the same blot ($n = 3$; *, $P < 0.05$; **, $P < 0.01$, one way ANOVA followed by Holm-Šídák method). Representative Western blots are presented. (C) Mice were treated with 30 mg/kg LDN/OSU-0212320 i.p. for 2 mo starting at 12 mo of age and were subjected to behavior tests (results shown in Fig. 6). After all behavior tests, PMVs were prepared from forebrains to determine EAAT2 protein levels by Western blot analysis. EAAT2 signal intensity was normalized to its actin signal intensity on the same blot ($n = 3$–4; *, $P < 0.05$, Student's t test). Representative Western blots are presented. All data are from three independent experiments. Mean ± SEM is shown.

EAAT2 mice to show better cognitive functions in these behavior tests compared with their WT littermates. Conclusively, these cognitive assessments indicate that restored EAAT2 protein function benefits cognitive functions.

To determine whether these cognitive-behavioral improvements were accompanied by restored synaptic integrity, we performed immunohistochemistry with synaptophysin antibodies. Synaptophysin is a presynaptic protein that has been widely used as a synaptic marker (Honer, 2003). Consistent with previous studies (Hsia et al., 1999; Mucke et al., 2000), a decrease in hippocampal synaptophysin immunoreactivity was observed in $APP_{Sw,Ind}$ mice. However, APP/EAAT2 mice exhibited restored synaptophysin immunoreactivity (representative images are shown in Fig. 3 E). Quantitative analysis of the CA3a region, which consists of mossy fiber terminals projected from the dentate gyrus and plays an important role in the encoding of new spatial information, indicated that APP/EAAT2 mice exhibit significantly higher synaptophysin immunoreactivity than APP mice (Fig. 3 E).

Furthermore, we examined amyloid deposition in young (6–9 mo) and older (12–15 mo) mice. Consistent with a previous study (Mucke et al., 2000), age-dependent Aβ plaque formation was detected in $APP_{Sw,Ind}$ mice by immunostaining with 6E10 antibodies. Fig. 3 F shows the quantitative results of the hippocampus regions, including CA1, CA3, and dentate gyrus, in older mice (12–15 mo). APP/EAAT2 mice exhibited significantly lowered plaque burden compared with their $APP_{Sw,Ind}$ littermates in all three regions. Representative images of the dentate gyrus region are shown in Fig. 3 F. These results suggest that restored EAAT2 protein function ameliorates amyloid deposition.

LDN/OSU-0212320 improved cognitive functions and reduced pathology in $APP_{Sw,Ind}$ mice

The aforementioned transgenic mice studies indicated that restored EAAT2 protein function benefits $APP_{Sw,Ind}$ mice. We then further investigated whether restored EAAT2 protein levels at symptomatic stages via a novel brain-penetrant compound, LDN/OSU-0212320 (Fig. 4 A), could provide therapeutic benefits in $APP_{Sw,Ind}$ mice. As mentioned previously, loss of EAAT2 protein in $APP_{Sw,Ind}$ mice is caused by disturbances at the posttranscriptional level because EAAT2 mRNA is not decreased; LDN/OSU-0212320 is capable of increasing EAAT2 expression through translational activation. Several preliminary experiments were conducted. First, to determine the optimal compound dosage, we assessed three different doses (10, 20, and 30 mg/kg) in 12-mo-old $APP_{Sw,Ind}$ mice. The results showed that EAAT2 protein levels were restored to normal levels at the dosage of 30 mg/kg by i.p. injection after 3-d daily treatment (Fig. 4 B). Second, although we have previously demonstrated the safety of this compound (Kong et al., 2014), we reconfirmed that long-term daily compound treatment at 30 mg/kg for 2 mo in $APP_{Sw,Ind}$ mice did not cause any abnormal behavior or body weight loss. Third, to determine an appropriate treatment

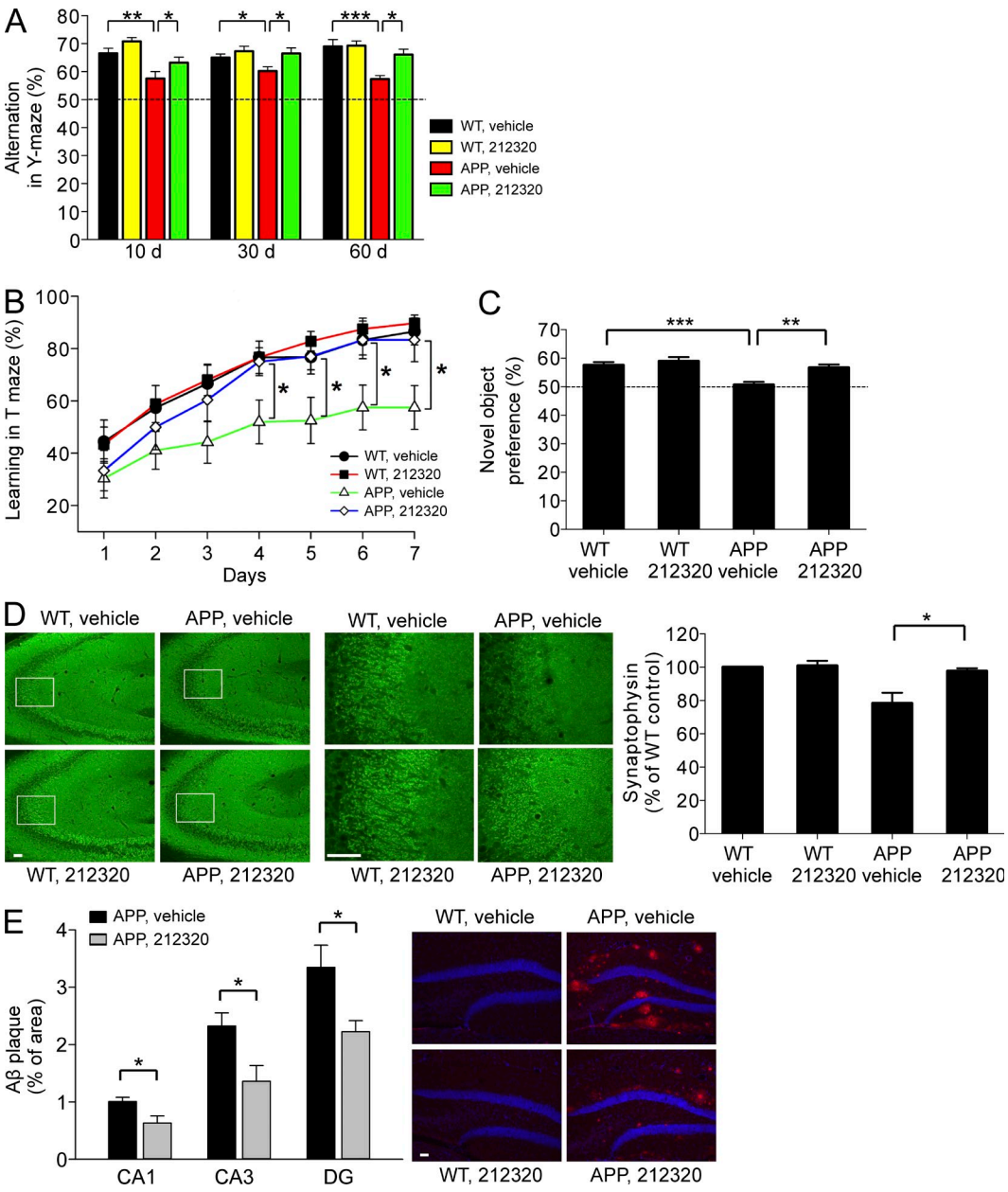

Figure 5. LDN/OSU-0212320–ameliorated memory deficits and pathology in 7-mo-old $APP_{Sw,Ind}$ mice. Mice were treated with 30 mg/kg LDN/OSU-0212320 i.p. starting at 7 mo of age. After 10 d of treatment, mice were subjected to Y-maze test, which was repeated after 30 d of treatment. After 60 d of treatment, mice underwent three cognitive tests (n = 18–24 per group) and then pathological experiments (n = 4 per group). (A) Y-maze tests assessing short-term memory (*, $P < 0.05$; **, $P < 0.01$; ***, $P < 0.001$, one way ANOVA followed by Holm-Šídák method). The dotted line represents the point at which mice did not remember the previously visited arm. (B) T-maze tests assessing spatial learning memory (*, $P < 0.05$, one-way repeated ANOVA followed by Student's t tests). (C) Novel object recognition tests assessing long-term nonspatial memory (**, $P < 0.01$; ***, $P < 0.001$, one way ANOVA followed by Holm-Šídák method). The dotted line represents the point at which mice did not remember the previous object. (D, left) Representative images of synaptophysin immunostaining in the CA3 region. The right micrographs show high-magnification images of the boxed areas in the left micrographs. (right) Quantitative analysis of synaptophysin immunoreactivity in the CA3a region indicated by the boxed areas (*, $P < 0.05$, Student's t test). (E, left) Quantitative analysis of Aβ immunostaining (*, $P < 0.05$, Student's t test). (right) Representative images of Aβ immunostaining in the dentate gyrus region are shown. Nuclei were stained with Hoechst 33342 (blue). (D and E) Bars, 50 µm. Data are from six (A–C) and three (D and E) independent experiments. Mean ± SEM is shown.

time, we evaluated cognitive functions by Y-maze, T-maze, and novel object recognition tests at 5 and 7 mo. Cognitive declines were already present by 5 mo and continued to progress at 7 mo. From these preliminary experiments, we determined that compound treatment starting at 7 mo and at 30 mg/kg would be most appropriate.

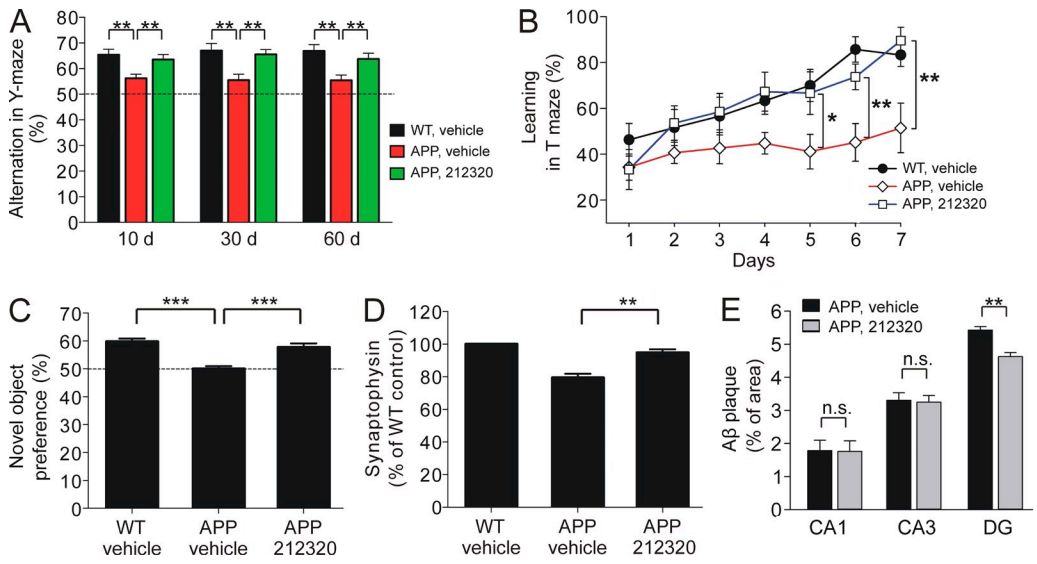

Figure 6. LDN/OSU-0212320–ameliorated memory deficits and pathology in 12-mo-old $APP_{Sw,Ind}$ mice. Mice were treated with 30 mg/kg LDN/OSU-0212320 i.p. starting at 12 mo of age. After 10 d of treatment, mice were subjected to Y-maze test, which was repeated after 30 d of treatment. After 60 d of treatment, mice underwent three cognitive tests (n = 18–21 per group) and then pathological experiments (n = 4 per group). (A) Y-maze tests assessing short-term memory (**, $P < 0.01$, one way ANOVA followed by Holm-Šídák method). The dotted line represents the point at which mice did not remember the previously visited arm. (B) T-maze tests assessing spatial learning memory (*, $P < 0.05$; **, $P < 0.01$, one-way repeated ANOVA followed by Student's t tests). (C) Novel object recognition tests assessing long-term nonspatial memory (***, $P < 0.001$, one way ANOVA followed by Holm-Šídák method). The dotted line represents the point at which mice did not remember the previous object. (D) Quantitative analysis of synaptophysin immunostaining in the CA3a region (**, $P < 0.01$, Student's t test). (E) Quantitative analysis of Aβ immunostaining (**, $P < 0.01$, Student's t test). Data are from four (A–C) and three (D and E) independent experiments. Mean ± SEM is shown.

Littermate-matched mice were divided into four groups: compound-treated $APP_{Sw,Ind}$, vehicle-treated $APP_{Sw,Ind}$, compound-treated WT, and vehicle-treated WT mice. Each group contained 18–24 mice with similar gender distribution. Mice were treated at the same time every day, starting at 7 mo, with 30 mg/kg of compound by i.p. injection. After 10 d of treatment, mice were subjected to short-term memory assessment by Y-maze, which was repeated after 30 d of treatment. After 60 d of treatment, mice underwent three cognitive tests, including Y-maze, T-maze, and novel object recognition tests. Examiners were blinded regarding treatment. After the behavioral test, mice were euthanized for pathological studies.

The results are presented in Fig. 5. Y-maze results demonstrated that short-term memory was restored after 10 d and continued to improve at 30 and 60 d after compound treatment (Fig. 5 A). T-maze results showed that spatial learning memory significantly improved after 60 d of treatment (Fig. 5 B). Novel object recognition test results also revealed significantly restored nonspatial long-term memory (Fig. 5 C). Notably, there were no obvious differences in compound effects between genders. In addition, we found that compound-treated WT mice exhibited better cognitive functions compared with that of their vehicle-treated littermates, and these findings were consistent with those observed in transgenic mice (Fig. 3).

Follow-up pathological experiments found that an increase in synaptophysin immunoreactivity, as assessed by immunostaining, was observed in the hippocampal CA3 region of compound-treated $APP_{Sw,Ind}$ mice but not in their $APP_{Sw,Ind}$ littermates treated with vehicle. Quantitative analysis of the CA3a region confirmed that compound-treated $APP_{Sw,Ind}$ mice exhibited significantly restored synaptophysin immunoreactivity (Fig. 5 D). Amyloid deposition was assessed by 6E10 antibodies. Results showed significantly lowered plaque burden in the hippocampal dentate gyrus as well as in the CA1 and CA3 subregions in compound-treated $APP_{Sw,Ind}$ mice as compared with $APP_{Sw,Ind}$ littermates treated with vehicle (Fig. 5 E).

To further investigate whether our compound could still provide benefits in older $APP_{Sw,Ind}$ mice, we performed similar behavioral and pathological experiments with compound treatment starting in 12-mo-old mice. Fig. 6 presents our findings, which were similar to the results we found in 7-mo-old mice. Specifically, compound-treated mice exhibited better cognitive functions across the Y-maze, T-maze, and novel object recognition tests (Fig. 6, A–C); additionally, it restored synaptic integrity (Fig. 6 D) and slightly reduced amyloid deposition in the dentate gyrus, but not in CA1 and CA3 subregions (Fig. 6 E). After all behavior tests, EAAT2 protein levels were measured, and the results showed that EAAT2 levels were restored in compound-treated mice (Fig. 4 C). Collectively, these behavioral and pathological findings indicate that LDN/OSU-0212320, which is capable of restoring EAAT2 protein levels, may serve as a potential therapeutic avenue.

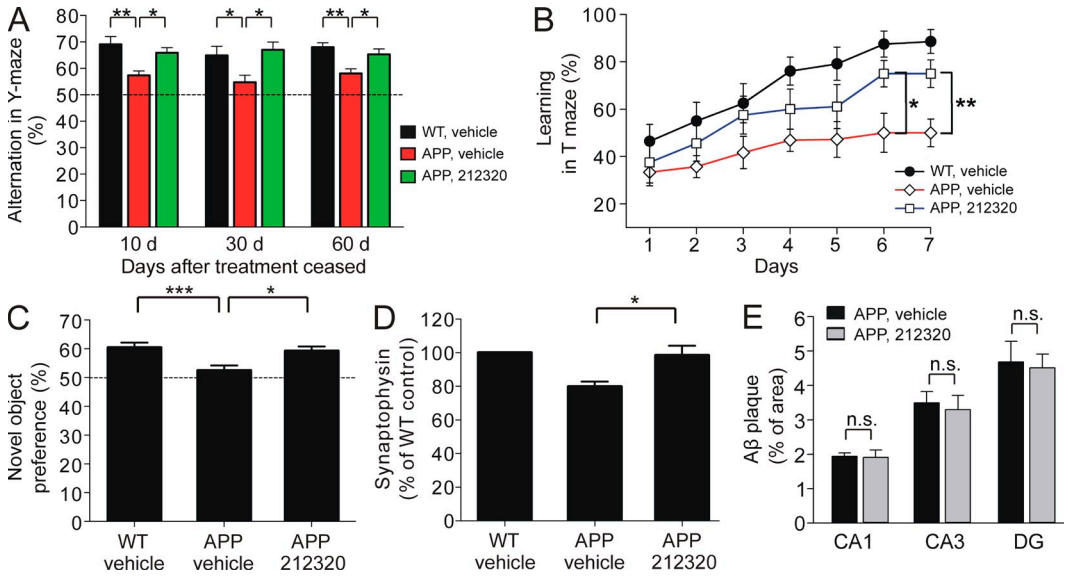

Figure 7. The beneficial effects of LDN/OSU-0212320 were sustained 1 mo after treatment was ceased. 12-mo-old mice were treated with 30 mg/kg LDN/OSU-0212320 i.p. for 2 mo and subjected to behavior tests (n = 10–11 mice per group) and pathological experiments (n = 4 mice per group) 1 mo after treatment cessation. (A) Y-maze assessment was measured 10, 20, and 30 d after treatment cessation (*, $P < 0.05$; **, $P < 0.01$, one way ANOVA followed by Holm-Šídák method). The dotted line represents the point at which mice did not remember the previously visited arm. (B) T-maze tests (*, $P < 0.05$; **, $P < 0.01$, one-way repeated ANOVA followed by Student's t tests). (C) Novel object recognition tests (*, $P < 0.05$; ***, $P < 0.001$, one way ANOVA followed by Holm-Šídák method). The dotted line represents the point at which mice did not remember the previous object. (D) Quantitative analysis of synaptophysin immunostaining in the CA3a region (*, $P < 0.05$, Student's t test). (E) Quantitative analysis of Aβ immunostaining. Data are from four (A–C) and three (D and E) independent experiments. Mean ± SEM is shown.

Beneficial effects of LDN/OSU-0212320 are sustained after 1-mo treatment cessation

To evaluate how long the benefits of treatment could last, 12-mo-old $APP_{Sw,Ind}$ mice were treated with LDN/OSU-0212320 for 2 mo and assessed for cognitive functions and pathology 1 mo after treatment was ceased. Y-maze assessment was measured 10, 20, and 30 d after treatment cessation and revealed sustained improved spatial short-term memory (Fig. 7 A). Improved spatial learning memory (T-maze test) and nonspatial long-term memory (novel object recognition test) were sustained 30 d after treatment was ceased, with gradual decline over time (Fig. 7, B and C). Consistently, synaptic integrity was also maintained 30 d after treatment (Fig. 7 D). However, amyloid deposition was not different between the two groups (Fig. 7 E). EAAT2 protein levels in compound-treated $APP_{Sw,Ind}$ mice returned to similar levels as that in $APP_{Sw,Ind}$ vehicle-treated mice in the absence of compound (not depicted). These results suggest that the observed beneficial effects are not palliative and that EAAT2 is a potential disease modifier for AD.

DISCUSSION

In the present study, we found that restored EAAT2 protein function attenuated premature death, memory loss, and AD-like pathology in $APP_{Sw,Ind}$ mice. These findings were solidly confirmed via a transgenic mouse and pharmacological approaches.

In our primary culture experiments (Fig. 1), we found that $A\beta_{25-35}$ caused severe neuronal damage and loss of EAAT2 in nontransgenic cultures, but not in transgenic cultures. Previous literature has demonstrated that Aβ can cause glutamate release, leading to excess glutamate-mediated neuronal damage, including synaptic loss (Chin et al., 2007; Kabogo et al., 2010; Talantova et al., 2013). Loss of synapses may make glutamate uptake unnecessary, thus down-regulating EAAT2. In EAAT2 transgenic cultures, increased EAAT2 levels can prevent excess glutamate-mediated toxicity and thus preserve synaptic integrity and EAAT2 protein levels. The cultures contained neurons that express EAAT3, type 1 astrocytes that express EAAT1, and type II astrocytes that express EAAT2. The population of type 1 astrocytes (EAAT1) in cultures is much higher than that of type 2 astrocytes (EAAT2). This is because differentiated type 2 astrocytes are not divided, but type 1 astrocytes continue dividing. The numbers of type 2 astrocytes are correlated with the numbers of neurons. Therefore, only ∼20% of glutamate uptake is inhibited by DHK. These cultures are appropriate for this study because they contain both neurons and type 2 astrocytes, which allowed us, as a first step, to assess whether increased EAAT2 protein expression could prevent Aβ-induced neuronal toxicity in vitro. The positive results from these experiments (Fig. 1) led us to move on with the in vivo transgenic mice and compound experiments (Figs. 2–7). We have previously used the primary neuron and astrocyte mixed cultures to demonstrate the protective effects of increased EAAT2 expression in glutamate-mediated toxicity in our EAAT2 transgenic mice study (Guo et al., 2003) and also in our compound LDN/OSU-0212320 study (Kong et al., 2014).

In our APP crossed EAAT2 mice experiments (Fig. 3), we found that APP/EAAT2 mice had significantly lowered premature death rates as compared with their APP littermates. This is probably caused by increased EAAT2 decreasing hyperexcitability. This possibility is currently under investigation. It is notable that we previously observed that increased EAAT2 protein expression provides significantly reduced seizure activity, neuronal death, and mortality rate in a pilocarpine-induced epilepsy model (Kong et al., 2012, 2014).

Furthermore, we found that APP/EAAT2 mice exhibited significantly improved cognitive functions and attenuated pathological changes. These beneficial effects are probably caused by reduced Aβ-mediated glutamate toxicity but not Aβ deposition. Notably, we found that increased EAAT2 was not able to decrease Aβ deposition in older mice as effectively as in younger mice (Figs. 5 E and 6 E). This suggests that EAAT2 may help prevent Aβ formation but cannot as adequately degrade preexisting Aβ deposition in older mice. Additionally, it was found that Aβ deposition does not contribute to restored memory (Fig. 7), suggesting that restored synapse integrity serves as a major player in memory restoration. Furthermore, we found that LDN/OSU-0212320 restored EAAT2 protein levels concomitant with improved synaptic integrity and cognitive functions. LDN/OSU-2123210 increases EAAT2 expression through the translational activation mechanism (Kong et al., 2014). It is possible that EAAT2 protein levels in perisynaptic processes of astrocytes are dependent on synaptic activity and are highly regulated at the translational level. Because synaptic plasticity is dynamic, translational regulation can more effectively respond to synaptic changes. This may be the reason why EAAT2 mRNA levels did not change in APP mice, whereas EAAT2 protein was down-regulated at the disease stage when significant synaptic loss occurred. Restoration of EAAT2 may prevent excess glutamate-mediated toxicity caused by Aβ. Additionally, it is possible that restored EAAT2 protein can reversely activate silent synapses to become active synapses. The detailed underlying mechanisms are currently being investigated.

Previous literature has indicated that EAAT2 plays an essential role in cognitive memory functions. As mentioned above, Mookherjee et al. (2011) reported accelerated cognitive deficits in AβPPswe/PS1ΔE9 mice as a consequence of EAAT2 protein loss. Bechtholt-Gompf et al. (2010) additionally reported that blocking EAAT2 glutamate uptake function by DHK impaired spatial memory. Furthermore, Pita-Almenar et al. (2012) reported increased glutamate uptake in hippocampal slides during early and late LTP. They demonstrated that EAAT2 is responsible for the increase in glutamate uptake during late LTP and that it may play an ongoing role in hippocampal circuitry to code and store information. Heo et al. (2012) also reported that increased EAAT2 complex levels were linked to spatial memory training during multiple T-maze tests. On a molecular level, Filosa et al. (2009) and Carmona et al. (2009) both reported that neuron–glia communication via EphA4/ephrin-A3 modulates LTP through glial glutamate transport. The studies suggested that EphA4/ephrin-A3 signaling is a critical mechanism for astrocytes to regulate synaptic function and plasticity. Moreover, Verbich et al. (2012) reported that EAAT2-mediated glutamate transport modulates dendritic spine head protrusions in the hippocampus and suggested that EAAT2 control of extracellular glutamate is important for spine head protrusion–mediated plasticity of spines. Based on our findings, we speculate that amyloid β–induced synaptic loss/dysfunction may lead to down-regulated EAAT2 protein expression at the translational level. Reactivating EAAT2 translation via LDN/OSU-0212320 restores synaptic plasticity and function, possibly through the EphA4/ephrin-A3 signaling pathway; this may account for the observed restored memory and learning functions in our compound-treated mice. This potential mechanism is currently under investigation.

Our data suggest that restored EAAT2 function is a potential new therapeutic approach for AD. Currently, clinical studies have focused on drugs that target the amyloid cascade. However, results from these studies have not yet yielded promising outcomes (Salomone et al., 2012; Tayeb et al., 2012). Our approach has several demonstrated advantages using LDN/OSU-0212320: (a) reverses memory and learning deficits after a short period of treatment, (b) sustains beneficial effects on cognitive functions even after 1 mo of treatment cessation, indicating a potential for disease modification, (c) restores synaptic integrity, and (d) increases EAAT2 expression via the translational rather than the transcriptional activation mechanism, which resolves the central problem of reduced EAAT2 expression. LDN/OSU-0212320 or its derivatives may have therapeutic potential for AD. Continued development of this compound series is currently under way.

MATERIALS AND METHODS

Animals. EAAT2 transgenic mice from a FVB/N mouse strain were previously generated in our laboratory (Guo et al., 2003). The EAAT2 transgene is driven by the human glial fibrillary acidic protein promoter. $APP_{Sw,Ind}$ transgenic mice (J20 mice, C57BL/6 mouse strain) were obtained from the laboratory of L. Mucke (The J. David Gladstone Institutes of San Francisco, San Francisco, CA). The APP/EAAT2 transgenic line was maintained by mating $APP_{Sw,Ind}$ males with EAAT2 females. Transgenes were determined by PCR using genomic DNA extracted from tail biopsies at 3 wk old with EAAT2 transgene–specific primers (5′-GGCAACTGGGGATGTACA-3′ and 5′-ACGCTGGGGAGTTTATTCAAGAAT-3′) and APP transgene–specific primers (5′-GGTGAGTTTGTAAGTGATGCC-3′ and 5′-TCTTCTTCTTCCACCTCAGC-3′). PCR conditions were as follows: for EAAT2, 94°C for 3 min, 94°C for 30 s, 55°C for 30 s, 72°C for 2 min for 30 cycles, followed by a 10-min extension at 72°C; for APP, 94°C for 90 s, 94°C for 30 s, 60°C for 45 s, 72°C for 45 s for 30 cycles, followed by 2-min extension at 72°C. Mice were housed in a 12-h light/dark cycle with free access to food and water. For compound treatment, mice received i.p. administration of LDN/OSU-0212320 at the indicated doses in 500 µl of 1% DMSO/1% polyethylene glycol 400/0.2% Tween 80/10% hydroxypropyl-β-cyclodextrin/saline. All experiments were approved by the Institutional Animal Care and Use Committee of The Ohio State University and the National Institutes of Health Guide for the Care and Use of Laboratory Animals.

Primary neuron and astrocyte mixed culture experiments. Primary dissociated neuron and astrocyte mixed cultures were prepared from the cortical brain of newborn (12–24 h) EAAT2 transgenic and nontransgenic pups as previously described (Guo et al., 2003). These cultures were maintained in DMEM

and supplemented with 0.5% fetal bovine serum, 100 μg/ml penicillin-streptomycin, and 1× B-27 (Invitrogen). 7-d-old cultures were used in this study. $A\beta_{25-35}$ (American Peptide) peptides were dissolved in water as previously described (Pike et al., 1993), and oligomers were confirmed as aggregate forms by Ponceau staining. 100 μM DHK (Sigma-Aldrich) was used to block EAAT2 function and added to the cultures 30 min before addition of $A\beta_{25-35}$. After 24 h of treatment, cultures were harvested for analyses. EAAT2 protein levels and glutamate uptake experiments are described below. For analyzing neuron morphology and number, cultures were fixed with 4% paraformaldehyde in 0.1 M PB (phosphate buffer), pH 7.4, permeabilized with 0.1% saponin in PBS for 20 min, blocked with 1% BSA in PBS/0.1% saponin for 30 min, and incubated with mouse anti-MAP2 antibodies (1:500; NeoMarker) in PBS containing 1% BSA overnight at 4°C. After washing with PBS containing 0.1% saponin, cells were incubated with Alexa Fluoro secondary antibodies and 1 μg/ml Hoechst 3342 (to visualize nuclear morphology) in PBS containing 1% BSA for 60 min, followed by thorough washing with PBS/0.1% saponin. Images were obtained using an Axioskop 2 upright microscope (Carl Zeiss) with AxioVision software (using Carl Zeiss 20×/0.5NA Plan-Neofluar). 15 fields (0.15 mm^2/field) per well were analyzed to determine total number of neurons, number of neurons with condensed nuclei, and intensity of MAP2 immunoreactivity. Each experiment was repeated three times. For MAP2 immunoreactivity, ImageJ 1.48b software (National Institutes of Health) was used to obtain the fluorescence intensity. For each experiment, the mean of immunoreactivity intensity from 15 fields of no $A\beta_{25-35}$ treatment (control) samples was arbitrarily set as 100%, and $A\beta_{25-35}$ treatment sample intensities were normalized to this control.

Immunoblot analysis. Immunoblotting was performed as described previously (Tian et al., 2010). In brief, the harvested samples from primary culture cells or plasma membrane vesicles (PMVs) prepared from forebrains were assayed for protein concentration, resolved by SDS-PAGE (8% polyacrylamide gel), and transferred onto nitrocellulose membranes. The following primary antibodies were used: rabbit anti-EAAT2 polyclonal antibodies (against the C terminus; 1:200) and goat anti-actin polyclonal antibodies (1:2,000; Santa Cruz Biotechnology, Inc.). The immunoreactive bands were detected using SuperSignal West Pico Chemiluminescent Substrate (Thermo Fisher Scientific) according to the manufacturer's directions. Band intensities were analyzed using ImageJ software.

[^{3}H]glutamate uptake assay. For primary culture experiments, we followed the procedures as reported previously (Tian et al., 2010). In brief, cells grown on 24-well plates were washed with sample buffer (320 mM sucrose in 50 mM Tris HCl, pH 7.4) and then incubated with Na^+-containing or Na^+-free Krebs buffer, which contains 0.125 μCi L-[^{3}H]glutamate (specific activity = 50.6 μCi/nmol; GE Healthcare) and 40 μM unlabeled glutamate, for 10 min at 37°C. Afterward, cells were washed with ice-cold 1× PBS and lysed in 1 mM NaOH. To distinguish DHK-sensitive [^{3}H]glutamate uptake from DHK-insensitive uptake, samples were incubated with 300 μM DHK (Sigma-Aldrich) 30 min before uptake.

For measuring the uptake of [^{3}H]glutamate into PMVs, we followed procedures as previously described (Guo et al., 2003). Mouse forebrain tissues were homogenized in sample buffer using a Dounce homogenizer and then centrifuged at 1,000 *g* for 10 min at 4°C. The supernatant (S1) was then centrifuged at 20,000 *g* for 30 min at 4°C, and the resultant PMV pellet (P2) was resuspended in either Na^+-containing or Na^+-free Krebs buffer. 100 μg PMV protein sample was used in each assay. The samples were incubated in 400 μl Na^+-containing or Na^+-free Krebs buffer, which contains 0.1 μCi L-[^{3}H]glutamate and 10 μM unlabeled glutamate, for 4 min at 37°C and then rapidly chilled on ice. The samples were then centrifuged at 20,000 *g* for 10 min at 4°C, and the pellets were rinsed with ice-cold 1× PBS and lysed in 1 mM NaOH. Each sample was measured three times. Three sets of mice were examined. To distinguish DHK-sensitive [^{3}H]glutamate uptake from DHK-insensitive uptake, samples were incubated with 300 μM DHK (Sigma-Aldrich) 30 min before uptake.

The amount of radiolabeled glutamate was measured using an LS6500 Multi-Purpose Scintillation Counter (counting efficiency for ^{3}H = 68%; Beckman Coulter). The amount of L-[^{3}H]glutamate uptake was calculated from the scintillation counting results using the following equation: [^{3}H]glutamate uptake (nmol) = (counts per minute/efficiency)/(2.22×10^6 disintegrations per minute/μCi)/(specific activity). Na^+-dependent L-[^{3}H]glutamate uptake was calculated by subtracting Na^+-independent L-[^{3}H]glutamate uptake (in Na^+-free Krebs buffer) from the total L-[^{3}H]glutamate uptake (in Na^+-containing Krebs buffer). DHK-sensitive L-[^{3}H]glutamate uptake was calculated by subtracting DHK-insensitive Na^+-dependent L-[^{3}H]glutamate uptake (DHK-treated sample) from total Na^+-dependent L-[^{3}H]glutamate uptake. The protein concentration was determined by the Bradford assay (Thermo Fisher Scientific). L-[^{3}H]glutamate uptake was represented as fmol/mg protein/min. Each value was made from the mean of triplicate data.

Y-maze test. The spontaneous alternation behavior of mice in a Y-maze was used to measure short-term memory deficits and motor activity in APP/EAAT2 mice. The maze apparatus consisted of three identical arms (35 × 5 × 10 cm) spaced at 120° apart and made of gray plastic. Each mouse was placed at the end of an arm and allowed to move freely throughout the maze during a 10-min session. An arm entry was recorded when a mouse moved all 4 ft into the arm. Motor activity was measured as the total number of arm entries. Short-term memory was measured as the percentage of spontaneous alternation. Alternation was defined as successive entries into the three arms on overlapping triplet sets. Spontaneous alternation (%) was calculated as the ratio of actual alternations to possible alternations, multiplied by 100, a method based on a previous study (Maurice et al., 1996).

T-maze test. To assess learning and memory deficits, the following procedure was performed: mice were maintained on a diet of 85% ad lib body weight to make the milk reward more appealing, and water was readily available. T-maze consisted of a 27 cm × 23 cm start box and a 30 cm × 11 cm start arm leading to two identical goal arms of 30 cm × 11 cm surrounded by a wall 10 cm high. A 35-mm plastic food dish was located 3 cm from the end of each goal arm. The maze was located on a table 1 m above the floor surrounded by a black board. The mice were first habituated to the maze for 3 d (3 min per mouse) and then habituated to a milk reward (2 ml of 50% sweetened, condensed milk). Next, mice were run through the maze three to five times each to determine their side preferences. Mice that demonstrated distinct side preferences only required three trials, whereas others required up to five trials. T-maze was measured for 9 d and consisted of four repeated trials with 60 min between trials. Mice were purposely trained against their side preferences with a milk reward in two steps: (1) a sample run in which the preferred side was blocked and the reward of 100 μl of 25% sweetened condensed milk was placed in the food dish at the end of the opposite arm and (2) a choice run in which the block was removed and mice were placed in the start arm with their backs facing the two choice arms and were free to choose the correct arm. The time interval between the sample and choice run was ∼5 s. Ideally, over time, the mice would learn to run to the arm containing the milk reward and learn against their side preferences. In the event that the mice went to the incorrect arm, the block was reapplied for 10 s, trapping the mice in the incorrect side without milk (as a form of punishment). Mice that directly and quickly went to the correct side containing the milk reward received a score of 1, and incorrect responses received a score of 0. The data are presented as the percentage of correct responses out of total number of responses. The examiner was blinded for genotype and treatment of mice.

Novel object recognition test. Novel object recognition tests based on the procedure of a previous study were performed, which consisted of a training phase and a testing phase (Stefanko et al., 2009). Mice were handled for at least 5 d to avoid stress, novelty of handling, and transport procedures. A plastic rectangular open field (35 × 45 × 30 cm) was used in balanced low-light conditions. The procedure consisted of three different phases: a habituation phase, an acquisition phase, and a retention phase. Mice were habituated to the experimental apparatus 15 min a day for two consecutive days in the absence of objects. During the acquisition phase, mice were placed in the

experimental apparatus with two identical objects (toy A & A′; 4 × 5 × 3 cm) and were allowed to explore for 10 min. The location of the object was counterbalanced. The objects and apparatus were thoroughly cleaned between trials to ensure that olfactory cues were not present. Retention was tested 24 h for long-term memory. During the retention phase, mice explored the experimental apparatus for 10 min in the presence of a familiar (toy A) and a novel object (toy B; 4 × 4 × 4 cm). Toy B was a distinct object with comparable manipulability and complexity made of the same type of material as toy A, and it was preapproved to have comparable attractiveness to another cohort of WT mice from the same strain. To determine the number of times that the mouse had visited the novel and familiar objects, all acquisition and retention trials were videotaped and analyzed independently by two individuals blind to treatment conditions and the genotype of subjects. A mouse was scored as exploring an object when its head was oriented toward the object within a distance of 1 cm or upon nose contact. N_{novel} refers to the total times that mice approached the novel object (toy B), and $N_{familiar}$ refers to the total times that mice approached toy A. The novel object recognition of toy B was expressed by $[B\% = N_{novel}/(N_{novel} + N_{familiar}) \times 100\%]$.

Immunohistochemistry. Mice were perfused transcardially with 4% paraformaldehyde in 0.1 M PB after being deeply anesthetized with 200 µl/10 g i.p. tribromoethanol (Avertin). Brains were rapidly dissected and stored in 4% paraformaldehyde for postfixation for 24 h, followed by cryoprotection with 30% sucrose for 72 h. 25-µm-thick coronal sections (−1.7 to −2.7 mm from Bregma for hippocampal analysis) were cut with a Microm cryostat at −20°C. Free floating brain sections were blocked in 5% normal goat serum (NGS; Vector Laboratories) with 0.2% Triton X-100 in Tris-buffered saline (TBS) for 60 min and incubated in specific antibodies overnight at 4°C. After thorough washing with TBS, sections were incubated with goat anti–rabbit or anti–mouse Alexa Fluoro secondary antibodies in TBST containing 2% NGS for 60 min, followed by thorough washing with TBS. The following antibodies were used: rabbit EAAT2 (1:200), mouse 6E10 (1:100; Covance), and mouse synaptophysin (1:1,000; EMD Millipore). Sections were washed thoroughly, mounted on glass slides, and cover-slipped with Immu-Mount (Thermo Fisher Scientific). Images were obtained using an Axioskop 2 upright microscope with AxioVision software (using Carl Zeiss 40×/0.75NA Plan-Neofluar and 10×/0.25NA Achroplan for synaptophysin immunostaining in the CA3 region, and Carl Zeiss 10×/0.25NA Achroplan for EAAT2 and Aβ immunostaining in the hippocampal dentate gyrus region). In addition, omission of primary antibodies resulted in a lack of immunoreactivity. The images of synaptophysin and 6E10 immunoreactivity for synaptic integrity and the Aβ deposition, respectively, were analyzed with ImageJ 1.48b software. For quantification of synaptophysin immunoreactivity on the CA3a region (Figs. 3 E, 5 D, 6 D, and 7 D), five to six images (in an area of 222 × 166 µm) from a series of sections for each mouse were collected. The signal intensities of these images were determined after subtracting background signals. The mean of these five to six signal intensities represents the mean signal intensity for each individual mouse. The number of animals used in each experiment is indicated in the figure legend. The mean intensity of WT samples was arbitrarily set as 100%, and the other samples were normalized to WT samples. For quantification of 6E10 immunoreactivity on the hippocampal regions (Figs. 3 F, 5 E, 6 E, and 7 E), 12 images (in an area of 888 × 666 µm) from a series of sections for each mouse were collected. The areas showing 6E10 immunoreactivity were determined based on a threshold value that was defined by the best discriminated staining from the background in each experiment. The mean of these 12 images represents the mean 6E10-labeled area for each individual mouse. The number of animals used in each experiment is indicated in the figure legend. The data are represented as a percentage of the 6E10-labeled area out of the total area.

Statistical analysis. The quantitative data in this study are expressed as the mean ± SEM. Premature death data were analyzed using χ^2 tests, which assessed for significant differences between $APP_{Sw,Ind}$ and APP/EAAT2 mice. T-maze test analysis was performed using repeated measures ANOVA followed by Student's *t* tests. To analyze Y-maze and novel object recognition for multiple group comparisons, data were analyzed by one-way ANOVAs and pairwise multiple comparisons by the Holm-Šídák method when data passed normality and equal variance tests. Immunostaining and glutamate uptake data were analyzed using two-tailed Student's *t* tests or ANOVA followed by Holm-Šídák method for data that passed normality and equal variance tests. The data were analyzed using Prism (GraphPad Software) or SigmaPlot. Values were considered significant at $P < 0.05$.

Online supplemental material. Table S1 shows glutamate uptake raw data. Online supplemental material is available at http://www.jem.org/cgi/content/full/jem.20140413/DC1.

We thank Dr. Lennart Mucke for providing $APP_{Sw,Ind}$ transgenic mice and Drs. Jeff Kuret and Douglas W. Scharre (The Ohio State University, Columbus, OH) for their advice on the present study.

This work was supported by US National Institutes of Health grants R01NS064275 and U01NS074601, the Thome Memorial Foundation, the Alzheimer's Association, the Indiana Alzheimer Disease Center, the BrightFocus Foundation, the Harvard NeuroDiscovery Center, and the Alzheimer's Drug Discovery Foundation.

The authors declare no competing financial interests.

Author contributions: K. Takahashi and Q. Kong designed and performed experiments and wrote the manuscript. Y. Lin performed experiments and edited the manuscript. N. Stouffer, D.A. Schulte, L. Lai, and S. Dominguez performed experiments. Q. Liu and L.-C. Chang gave technical support and conceptual advice. X. Xing, G.D. Cuny, K.J. Hodgetts, and M.A. Glicksman generated compounds, participated in study design, and edited the manuscript. C.-L.G. Lin designed and supervised the study and edited the manuscript.

Submitted: 3 March 2014
Accepted: 27 January 2015

REFERENCES

Bechtholt-Gompf, A.J., H.V. Walther, M.A. Adams, W.A. Carlezon Jr., D. Ongür, and B.M. Cohen. 2010. Blockade of astrocytic glutamate uptake in rats induces signs of anhedonia and impaired spatial memory. *Neuropsychopharmacology*. 35:2049–2059. http://dx.doi.org/10.1038/npp.2010.74

Bell, K.F., D.A. Bennett, and A.C. Cuello. 2007. Paradoxical upregulation of glutamatergic presynaptic boutons during mild cognitive impairment. *J. Neurosci.* 27:10810–10817. http://dx.doi.org/10.1523/JNEUROSCI.3269-07.2007

Bordji, K., J. Becerril-Ortega, O. Nicole, and A. Buisson. 2010. Activation of extrasynaptic, but not synaptic, NMDA receptors modifies amyloid precursor protein expression pattern and increases amyloid-β production. *J. Neurosci.* 30:15927–15942. http://dx.doi.org/10.1523/JNEUROSCI.3021-10.2010

Braak, H., and E. Braak. 1998. Evolution of neuronal changes in the course of Alzheimer's disease. *J. Neural Transm. Suppl.* 53:127–140. http://dx.doi.org/10.1007/978-3-7091-6467-9_11

Carmona, M.A., K.K. Murai, L. Wang, A.J. Roberts, and E.B. Pasquale. 2009. Glial ephrin-A3 regulates hippocampal dendritic spine morphology and glutamate transport. *Proc. Natl. Acad. Sci. USA*. 106:12524–12529. http://dx.doi.org/10.1073/pnas.0903328106

Chaudhry, F.A., K.P. Lehre, M. van Lookeren Campagne, O.P. Ottersen, N.C. Danbolt, and J. Storm-Mathisen. 1995. Glutamate transporters in glial plasma membranes: highly differentiated localizations revealed by quantitative ultrastructural immunocytochemistry. *Neuron*. 15:711–720. http://dx.doi.org/10.1016/0896-6273(95)90158-2

Chin, J.H., L. Ma, D. MacTavish, and J.H. Jhamandas. 2007. Amyloid β protein modulates glutamate-mediated neurotransmission in the rat basal forebrain: involvement of presynaptic neuronal nicotinic acetylcholine and metabotropic glutamate receptors. *J. Neurosci.* 27:9262–9269. http://dx.doi.org/10.1523/JNEUROSCI.1843-07.2007

Colton, C.K., Q. Kong, L. Lai, M.X. Zhu, K.I. Seyb, G.D. Cuny, J. Xian, M.A. Glicksman, and C.L. Lin. 2010. Identification of translational activators of

glial glutamate transporter EAAT2 through cell-based high-throughput screening: an approach to prevent excitotoxicity. *J. Biomol. Screen.* 15:653–662. http://dx.doi.org/10.1177/1087057110370998

Filosa, A., S. Paixão, S.D. Honsek, M.A. Carmona, L. Becker, B. Feddersen, L. Gaitanos, Y. Rudhard, R. Schoepfer, T. Klopstock, et al. 2009. Neuron-glia communication via EphA4/ephrin-A3 modulates LTP through glial glutamate transport. *Nat. Neurosci.* 12:1285–1292. http://dx.doi.org/10.1038/nn.2394

Francis, P.T. 2003. Glutamatergic systems in Alzheimer's disease. *Int. J. Geriatr. Psychiatry.* 18:S15–S21. http://dx.doi.org/10.1002/gps.934

Friedman, D., L.S. Honig, and N. Scarmeas. 2012. Seizures and epilepsy in Alzheimer's disease. *CNS Neurosci. Ther.* 18:285–294. http://dx.doi.org/10.1111/j.1755-5949.2011.00251.x

Guo, H., L. Lai, M.E. Butchbach, M.P. Stockinger, X. Shan, G.A. Bishop, and C.L. Lin. 2003. Increased expression of the glial glutamate transporter EAAT2 modulates excitotoxicity and delays the onset but not the outcome of ALS in mice. *Hum. Mol. Genet.* 12:2519–2532. http://dx.doi.org/10.1093/hmg/ddg267

Heo, S., G. Jung, T. Beuk, H. Höger, and G. Lubec. 2012. Hippocampal glutamate transporter 1 (GLT-1) complex levels are paralleling memory training in the Multiple T-maze in C57BL/6J mice. *Brain Struct. Funct.* 217:363–378. http://dx.doi.org/10.1007/s00429-011-0362-5

Honer, W.G. 2003. Pathology of presynaptic proteins in Alzheimer's disease: more than simple loss of terminals. *Neurobiol. Aging.* 24:1047–1062. http://dx.doi.org/10.1016/j.neurobiolaging.2003.04.005

Hsia, A.Y., E. Masliah, L. McConlogue, G.Q. Yu, G. Tatsuno, K. Hu, D. Kholodenko, R.C. Malenka, R.A. Nicoll, and L. Mucke. 1999. Plaque-independent disruption of neural circuits in Alzheimer's disease mouse models. *Proc. Natl. Acad. Sci. USA.* 96:3228–3233. http://dx.doi.org/10.1073/pnas.96.6.3228

Hsiao, K.K., D.R. Borchelt, K. Olson, R. Johannsdottir, C. Kitt, W. Yunis, S. Xu, C. Eckman, S. Younkin, D. Price, et al. 1995. Age-related CNS disorder and early death in transgenic FVB/N mice overexpressing Alzheimer amyloid precursor proteins. *Neuron.* 15:1203–1218. http://dx.doi.org/10.1016/0896-6273(95)90107-8

Jacob, C.P., E. Koutsilieri, J. Bartl, E. Neuen-Jacob, T. Arzberger, N. Zander, R. Ravid, W. Roggendorf, P. Riederer, and E. Grünblatt. 2007. Alterations in expression of glutamatergic transporters and receptors in sporadic Alzheimer's disease. *J. Alzheimers Dis.* 11:97–116.

Kabogo, D., G. Rauw, A. Amritraj, G. Baker, and S. Kar. 2010. β-amyloid-related peptides potentiate K^+-evoked glutamate release from adult rat hippocampal slices. *Neurobiol. Aging.* 31:1164–1172. http://dx.doi.org/10.1016/j.neurobiolaging.2008.08.009

Kashani, A., E. Lepicard, O. Poirel, C. Videau, J.P. David, C. Fallet-Bianco, A. Simon, A. Delacourte, B. Giros, J. Epelbaum, et al. 2008. Loss of VGLUT1 and VGLUT2 in the prefrontal cortex is correlated with cognitive decline in Alzheimer disease. *Neurobiol. Aging.* 29:1619–1630. http://dx.doi.org/10.1016/j.neurobiolaging.2007.04.010

Kim, S.H., P.E. Fraser, D. Westaway, P.H. St George-Hyslop, M.E. Ehrlich, and S. Gandy. 2010. Group II metabotropic glutamate receptor stimulation triggers production and release of Alzheimer's amyloid β_{42} from isolated intact nerve terminals. *J. Neurosci.* 30:3870–3875. http://dx.doi.org/10.1523/JNEUROSCI.4717-09.2010

Kirvell, S.L., M. Esiri, and P.T. Francis. 2006. Down-regulation of vesicular glutamate transporters precedes cell loss and pathology in Alzheimer's disease. *J. Neurochem.* 98:939–950. http://dx.doi.org/10.1111/j.1471-4159.2006.03935.x

Kong, Q., K. Takahashi, D. Schulte, N. Stouffer, Y. Lin, and C.L. Lin. 2012. Increased glial glutamate transporter EAAT2 expression reduces epileptogenic processes following pilocarpine-induced status epilepticus. *Neurobiol. Dis.* 47:145–154. http://dx.doi.org/10.1016/j.nbd.2012.03.032

Kong, Q., L.C. Chang, K. Takahashi, Q. Liu, D.A. Schulte, L. Lai, B. Ibabao, Y. Lin, N. Stouffer, C. Das Mukhopadhyay, et al. 2014. Small-molecule activator of glutamate transporter EAAT2 translation provides neuroprotection. *J. Clin. Invest.* 124:1255–1267. http://dx.doi.org/10.1172/JCI66163

Lesné, S., C. Ali, C. Gabriel, N. Croci, E.T. MacKenzie, C.G. Glabe, M. Plotkine, C. Marchand-Verrecchia, D. Vivien, and A. Buisson. 2005. NMDA receptor activation inhibits α-secretase and promotes neuronal amyloid-β production. *J. Neurosci.* 25:9367–9377. http://dx.doi.org/10.1523/JNEUROSCI.0849-05.2005

Li, S., M. Mallory, M. Alford, S. Tanaka, and E. Masliah. 1997. Glutamate transporter alterations in Alzheimer disease are possibly associated with abnormal APP expression. *J. Neuropathol. Exp. Neurol.* 56:901–911. http://dx.doi.org/10.1097/00005072-199708000-00008

Li, S., S. Hong, N.E. Shepardson, D.M. Walsh, G.M. Shankar, and D. Selkoe. 2009. Soluble oligomers of amyloid β protein facilitate hippocampal long-term depression by disrupting neuronal glutamate uptake. *Neuron.* 62:788–801. http://dx.doi.org/10.1016/j.neuron.2009.05.012

Li, S., M. Jin, T. Koeglsperger, N.E. Shepardson, G.M. Shankar, and D.J. Selkoe. 2011. Soluble Aβ oligomers inhibit long-term potentiation through a mechanism involving excessive activation of extrasynaptic NR2B-containing NMDA receptors. *J. Neurosci.* 31:6627–6638. http://dx.doi.org/10.1523/JNEUROSCI.0203-11.2011

Lin, C.L., Q. Kong, G.D. Cuny, and M.A. Glicksman. 2012. Glutamate transporter EAAT2: a new target for the treatment of neurodegenerative diseases. *Future Med. Chem.* 4:1689–1700. http://dx.doi.org/10.4155/fmc.12.122

Masliah, E., M. Alford, R. DeTeresa, M. Mallory, and L. Hansen. 1996. Deficient glutamate transport is associated with neurodegeneration in Alzheimer's disease. *Ann. Neurol.* 40:759–766. http://dx.doi.org/10.1002/ana.410400512

Maurice, T., B.P. Lockhart, and A. Privat. 1996. Amnesia induced in mice by centrally administered beta-amyloid peptides involves cholinergic dysfunction. *Brain Res.* 706:181–193. http://dx.doi.org/10.1016/0006-8993(95)01032-7

Minkeviciene, R., S. Rheims, M.B. Dobszay, M. Zilberter, J. Hartikainen, L. Fülöp, B. Penke, Y. Zilberter, T. Harkany, A. Pitkänen, and H. Tanila. 2009. Amyloid β-induced neuronal hyperexcitability triggers progressive epilepsy. *J. Neurosci.* 29:3453–3462. http://dx.doi.org/10.1523/JNEUROSCI.5215-08.2009

Mookherjee, P., P.S. Green, G.S. Watson, M.A. Marques, K. Tanaka, K.D. Meeker, J.S. Meabon, N. Li, P. Zhu, V.G. Olson, and D.G. Cook. 2011. GLT-1 loss accelerates cognitive deficit onset in an Alzheimer's disease animal model. *J. Alzheimers Dis.* 26:447–455.

Mucke, L., E. Masliah, G.Q. Yu, M. Mallory, E.M. Rockenstein, G. Tatsuno, K. Hu, D. Kholodenko, K. Johnson-Wood, and L. McConlogue. 2000. High-level neuronal expression of abeta 1-42 in wild-type human amyloid protein precursor transgenic mice: synaptotoxicity without plaque formation. *J. Neurosci.* 20:4050–4058.

Palop, J.J., J. Chin, E.D. Roberson, J. Wang, M.T. Thwin, N. Bien-Ly, J. Yoo, K.O. Ho, G.Q. Yu, A. Kreitzer, et al. 2007. Aberrant excitatory neuronal activity and compensatory remodeling of inhibitory hippocampal circuits in mouse models of Alzheimer's disease. *Neuron.* 55:697–711. http://dx.doi.org/10.1016/j.neuron.2007.07.025

Pike, C.J., D. Burdick, A.J. Walencewicz, C.G. Glabe, and C.W. Cotman. 1993. Neurodegeneration induced by beta-amyloid peptides in vitro: the role of peptide assembly state. *J. Neurosci.* 13:1676–1687.

Pita-Almenar, J.D., S. Zou, C.M. Colbert, and A. Eskin. 2012. Relationship between increase in astrocytic GLT-1 glutamate transport and late-LTP. *Learn. Mem.* 19:615–626. http://dx.doi.org/10.1101/lm.023259.111

Rothstein, J.D., M. Dykes-Hoberg, C.A. Pardo, L.A. Bristol, L. Jin, R.W. Kuncl, Y. Kanai, M.A. Hediger, Y. Wang, J.P. Schielke, and D.F. Welty. 1996. Knockout of glutamate transporters reveals a major role for astroglial transport in excitotoxicity and clearance of glutamate. *Neuron.* 16:675–686. http://dx.doi.org/10.1016/S0896-6273(00)80086-0

Salomone, S., F. Caraci, G.M. Leggio, J. Fedotova, and F. Drago. 2012. New pharmacological strategies for treatment of Alzheimer's disease: focus on disease modifying drugs. *Br. J. Clin. Pharmacol.* 73:504–517. http://dx.doi.org/10.1111/j.1365-2125.2011.04134.x

Scott, H.A., F.M. Gebhardt, A.D. Mitrovic, R.J. Vandenberg, and P.R. Dodd. 2011. Glutamate transporter variants reduce glutamate uptake in Alzheimer's disease. *Neurobiol. Aging.* 32:553.e1–553.e11. http://dx.doi.org/10.1016/j.neurobiolaging.2010.03.008

Shankar, G.M., S. Li, T.H. Mehta, A. Garcia-Munoz, N.E. Shepardson, I. Smith, F.M. Brett, M.A. Farrell, M.J. Rowan, C.A. Lemere, et al.

2008. Amyloid-β protein dimers isolated directly from Alzheimer's brains impair synaptic plasticity and memory. *Nat. Med.* 14:837–842. http://dx.doi.org/10.1038/nm1782

Sokolow, S., S.H. Luu, K. Nandy, C.A. Miller, H.V. Vinters, W.W. Poon, and K.H. Gylys. 2012. Preferential accumulation of amyloid-beta in presynaptic glutamatergic terminals (VGluT1 and VGluT2) in Alzheimer's disease cortex. *Neurobiol. Dis.* 45:381–387. http://dx.doi.org/10.1016/j.nbd.2011.08.027

Stefanko, D.P., R.M. Barrett, A.R. Ly, G.K. Reolon, and M.A. Wood. 2009. Modulation of long-term memory for object recognition via HDAC inhibition. *Proc. Natl. Acad. Sci. USA.* 106:9447–9452. http://dx.doi.org/10.1073/pnas.0903964106

Talantova, M., S. Sanz-Blasco, X. Zhang, P. Xia, M.W. Akhtar, S. Okamoto, G. Dziewczapolski, T. Nakamura, G. Cao, A.E. Pratt, et al. 2013. Aβ induces astrocytic glutamate release, extrasynaptic NMDA receptor activation, and synaptic loss. *Proc. Natl. Acad. Sci. USA.* 110:E2518–E2527. http://dx.doi.org/10.1073/pnas.1306832110

Tayeb, H.O., H.D. Yang, B.H. Price, and F.I. Tarazi. 2012. Pharmacotherapies for Alzheimer's disease: beyond cholinesterase inhibitors. *Pharmacol. Ther.* 134:8–25. http://dx.doi.org/10.1016/j.pharmthera.2011.12.002

Tian, G., Q. Kong, L. Lai, A. Ray-Chaudhury, and C.L. Lin. 2010. Increased expression of cholesterol 24S-hydroxylase results in disruption of glial glutamate transporter EAAT2 association with lipid rafts: a potential role in Alzheimer's disease. *J. Neurochem.* 113:978–989. http://dx.doi.org/10.1111/j.1471-4159.2010.06661.x

Verbich, D., G.A. Prenosil, P.K. Chang, K.K. Murai, and R.A. McKinney. 2012. Glial glutamate transport modulates dendritic spine head protrusions in the hippocampus. *Glia.* 60:1067–1077. http://dx.doi.org/10.1002/glia.22335

Verret, L., E.O. Mann, G.B. Hang, A.M. Barth, I. Cobos, K. Ho, N. Devidze, E. Masliah, A.C. Kreitzer, I. Mody, et al. 2012. Inhibitory interneuron deficit links altered network activity and cognitive dysfunction in Alzheimer model. *Cell.* 149:708–721. http://dx.doi.org/10.1016/j.cell.2012.02.046

Wang, Q., D.M. Walsh, M.J. Rowan, D.J. Selkoe, and R. Anwyl. 2004. Block of long-term potentiation by naturally secreted and synthetic amyloid β-peptide in hippocampal slices is mediated via activation of the kinases c-Jun N-terminal kinase, cyclin-dependent kinase 5, and p38 mitogen-activated protein kinase as well as metabotropic glutamate receptor type 5. *J. Neurosci.* 24:3370–3378. http://dx.doi.org/10.1523/JNEUROSCI.1633-03.2004

Xing, X., L.C. Chang, Q. Kong, C.K. Colton, L. Lai, M.A. Glicksman, C.L. Lin, and G.D. Cuny. 2011. Structure-activity relationship study of pyridazine derivatives as glutamate transporter EAAT2 activators. *Bioorg. Med. Chem. Lett.* 21:5774–5777. http://dx.doi.org/10.1016/j.bmcl.2011.08.009